16

Quantum Confinement in Heterostructured Semiconductor Nanowires with Graded Interfaces

G. A. Farias, J. S. de Sousa and A. Chaves
Universidade Federal do Ceará
Brazil

1. Theoretical model for wires with graded interfaces

In a simple approximation, quantum wires can be modeled by cylinders composed by two semiconductor materials with different energy gaps, A and B, as shown in Fig. 1 (a) and (b), for block-by-block and core-shell wires, respectively. In both cases, the existence of smooth interfaces with thickness w between materials is considered, by assuming that the composition χ of the alloy $A_\chi B_{1-\chi}$ varies linearly in the interfacial region. The heterostructure potential depends on χ as $V^{het}(\vec{r}) = e_1\chi(\vec{r}) + e_2\chi^2(\vec{r})$, where e_1 and e_2 are interpolation parameters (Li, 2000), whereas the effective mass is given by a linear interpolation $m(\vec{r}) = m_A\chi(\vec{r}) + (1-\chi(\vec{r}))m_B$, with $m_{A(B)}$ as the effective mass of the material A (B). In Fig. 1 (a), the wire is *free-standing, i. e.*, not embedded in a matrix of another material, consequently, an infinite potential can be assumed for the external region.

In cylindrical coordinates, the inclusion of a magnetic-field $\vec{B} = B\hat{z}$ into the Hamiltonian is made through the symmetric gauge vector potential $\vec{A} = 1/2\,B\rho\hat{\theta}$. In addition, for all cases that will be discussed, our system presents circular symmetry, so that a solution $exp[il\theta]$, with $l = 0, \pm 1, \pm 2, \ldots$, is appropriate for the angular coordinate. Thus, for the general case where both the effective mass and the potential depend on the spatial coordinates, the Schrödinger equation, within the effective-mass approximation, describing the confinement of each carrier in QWR reads

$$\left\{-\frac{\hbar^2}{2}\left[\frac{1}{\rho}\frac{d}{d\rho}\frac{\rho}{m^{\|}(\vec{r})}\frac{d}{d\rho}+\frac{\partial}{\partial z}\frac{1}{m^{\perp}(\vec{r})}\frac{\partial}{\partial z}\right]+\frac{m^{\|}(\vec{r})\omega_c^2\rho^2}{8}+\frac{\hbar^2 l^2}{2m^{\|}(\vec{r})\rho^2}+\frac{l}{2}\hbar\omega_c+V(\vec{r})\right\}\Psi(\vec{r})=E\Psi(\vec{r}) \quad (1)$$

Where $m^{\|}$ and $m^{\perp}$ are the in-plane and longitudinal effective masses, respectively, and $\omega_c = eB/m^{\|}$ is the cyclotron frequency. In core-shell wires, we consider a potential V which includes not only the heterostructure, but also the electron-hole Coulomb potential. For the zinc-blend materials we studied, the valence band presents heavy and light hole states and, since in block-by-block wires the charge carriers are confined in three dimensions, the valence band states cannot be discussed in terms of a single hole state and a multi-band k.p study is necessary in this case. Hence, in this work we study excitonic effects only for core-

Source: Nanowires, Book edited by: Paola Prete,
ISBN 978-953-7619-79-4, pp. 414, March 2010, INTECH, Croatia, downloaded from SCIYO.COM

shell wires, and the investigation of the exciton energies in wires with longitudinal heterostructures is left as subject for future research.

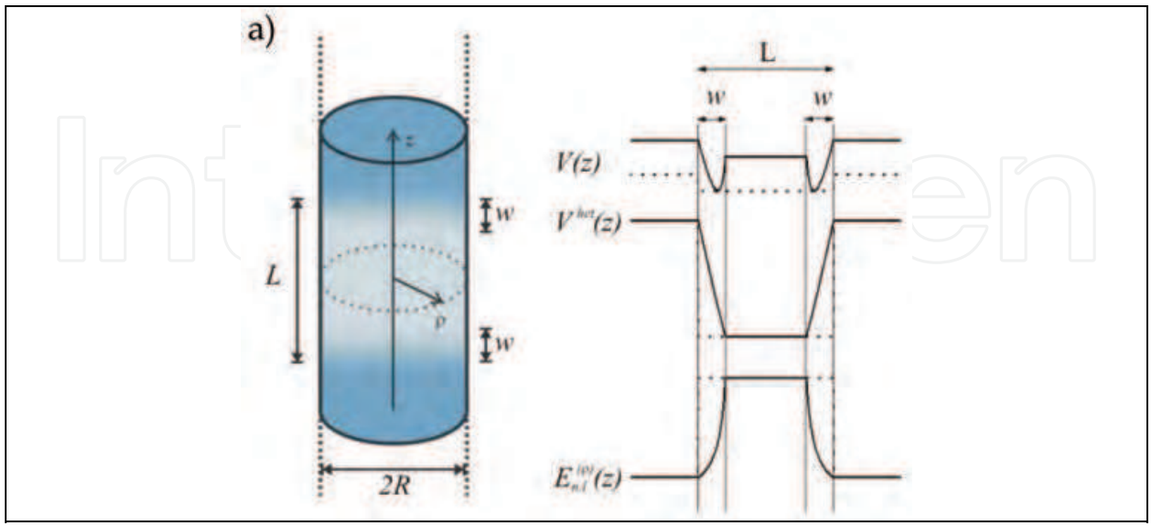

Fig. 1. (a) Sketch of our model of block-by-block quantum wires: the wire radius is R and a longitudinal heterostructured is considered in *z* direction; darker and lighter regions represent different materials and a smooth interface of thickness *w* between them is considered. A scheme of the effective potential in *z* is depicted for abrupt (dotted) and non-abrupt (solid) interfaces (see explanation in the text). (b) Sketch for the core-shell and core-multi-shell quantum wires considered in this work.

2. Longidudinal heterostructures

In this case, we consider a circular cylindrical quantum wire at an infinite potential region with a longitudinal block-by-block heterostructure. After a separation of variables $\Psi(\vec{r}) = \left(1/\sqrt{2\pi}\right)\exp[il\theta]R(r)Z(z)$, the Schrödinger equation for the radial confinement of one electron in this system, in the presence of an axial magnetic field, is obtained from Eq. (1) as

$$\left[-\frac{\hbar^2}{2m^{\|}(z)\rho}\frac{d}{d\rho}\rho\frac{d}{d\rho}+\frac{m^{\|}(z)\omega_c^2}{8}+\frac{\hbar^2 l^2}{2m^{\|}(z)\rho^2}+\frac{l}{2}\hbar\omega_c\right]R(\rho)=E^{(\rho)}R(\rho) \qquad (2)$$

where the effective mass depends only on *z*, due to the existence of a heterostructure in this direction. In the absence of magnetic fields, it is straightforwardly verified that Eq. (2) becomes the Bessel equation, so that the eigenfunctions are given by the Bessel functions which do not diverge in the origin $J_l(k\rho)$, where $k=\sqrt{2m^{\|}(z)E_l^{(\rho)}/\hbar^2}$. The boundary condition at $\rho = R$, where an infinite potential is considered, implies that $J_l(kR)=0$, which leads to the quantization condition $k_{n,l}=x_{n,l}/R$, where $x_{n,l}$ is the *n*-th root of the Bessel funcion of order *l*. Hence, the radial confinement energies are easily analytically found as $E_{n,l}^{(\rho)}(z)=\hbar^2 x_{n,l}^2/2m^{\|}(z)R^2$.

In the presence of a magnetic field, analytical solutions for Eq. (2) can be found as well, not in terms of Bessel functions, but as Kummer functions instead. First, let us make the change of variables $\xi = \rho^2/2a_c$, where $a_c = \sqrt{\hbar/eB}$ is the cyclotron radius. Equation (2) now reads

$$\left[\xi\frac{d^2}{d\xi^2}+\frac{d}{d\xi}-\left(\frac{l}{2}+\frac{l^2}{4\xi}+\frac{\xi}{4}-\frac{E}{\hbar\omega_c}\right)\right]R(\xi)=0 \tag{3}$$

Taking account of the polynomial and assymptotic behaviors of $R(\xi)$, it is reasonable to try a solution of the form $R(\xi)=\xi^{|l|/2}e^{-\xi/2}F(\xi)$. With this solution, Eq. (3) is rewritten as

$$\xi\frac{d^2F(\xi)}{d\xi^2}+\left[(|l|+1)-\xi\right]\frac{dF(\xi)}{d\xi}-\left(\frac{l}{2}+\frac{|l|}{2}+\frac{1}{2}-\frac{E}{\hbar\omega_c}\right)F(\xi)=0 \tag{4}$$

Equation (4) is identified as a confluent hypergeometric differential equation, which can be solved in terms of the Kummer function of the first kind $F_1(\alpha,\beta,\xi)$, which remains finite in the origin. The eigenfunctions are then given by $R_{n,l}(\xi)=N\xi^{|l|/2}e^{-\xi/2}F_1(\alpha,|l|+1,\xi)$, where N is a normalization parameter and $\alpha = l/2+|l|/2+1/2-E/\hbar\omega_c$. The boundary condition at $\rho = R$ now leads to $F_1(\alpha,|l|+1,\xi_R)=0$, so that $\alpha = x_{n,|l|}$ must be the n-th zero of $F_1(\alpha,|l|+1,R^2/2a_c)=0$. Finally, the radial confinement energy in the presence of a magnetic field is written as

$$E_{n,l}^{(\rho)}(z)=\hbar\omega_c(z)\left(x_{n,|l|}+\frac{l}{2}+\frac{|l|}{2}+\frac{1}{2}\right) \tag{5}$$

Notice that this energy depends on z, for the effective mass is different for each material. Consequently, this energy can be viewed as an additional potential in this direction, which is summed up to the heterostructure potential V^{het}, leading to an effective potential $V(z)=V^{het}(z)+E_{n,l}^{(\rho)}(z)$. The effective potential $V(z)$ is then adjusted so that the energy referential is at the GaP (InP) layers.The shape of this effective potential is illustrated as dashed and solid curves in Fig. 1 (a), for abrupt and smooth interfaces, respectively. The radial confinement energy $E_{n,l}^{(\rho)}$ depends on the inverse of the effective mass and, since the electron effective masses at GaAs and InAs are lighter than those at GaP and InP, (Li, 2000) this energy exhibits a barrier-like profile as a function of z in GaP/GaAs/GaP or InP/InAs/InP heterostructures. For abrupt interfaces (dashed), when this energy is summed to the heterostructure potential, depending on the wire radius, the effective potential $V(z)$ can end up i) with a lower effective band offset, ii) with an inversion of the carriers localization, as in a type-II structure, or even iii) with a zero effective band offset, so that a carrier would behave like a free particle in z-direction, despite the presence of the longitudinal heterostructure (Voon & Willatzen, 2003). When graded interfaces are taken into account (solid), the effective potential at the interfacial region exhibits a peculiar shape, with cusps that are able to confine the carriers in this region. In the following results of this

section, we will show the effects of this interfacial confinement on the energy states, as well as on the transport properties of longitudinally heterostructured QWR.

2.1 Single heterostructure

The parameters for the materials that compose the heterostructures are assumed as m_{GaAs} = 0.063m_0 (m_{InAs} = 0.027m_0) and m_{GaP} = 0.33m_0 (m_{InP} = 0.077m_0) for electron effective masses, e_1 = 1.473 eV and e_2 = 0.146 eV (e_1 = 1.083 eV and e_2 = 0.091 eV) for the interpolation parameters and the conduction band offset is assumed as Q_e = 0.5 (Q_e = 0.68), for GaP/GaAs (InP/InAs) heterostructures. (Li, 2000)

Figure 2 shows the confinement energies E_e of electrons in the absence of magnetic fields, for states with the set of quantum numbers (n, l, m) as (1, 0, 1) (symbols) and (1, 1, 1) (curves) in a GaP/GaAs QWR, as a function of the well width L, formed by the longitudinal heterostructure. The interface thickness between materials was considered as (a) w = 0 Å and (b) 20 Å, and two values for the wire radius are chosen, in order to observe the effect of enhancing the radial confinements on the energy levels.

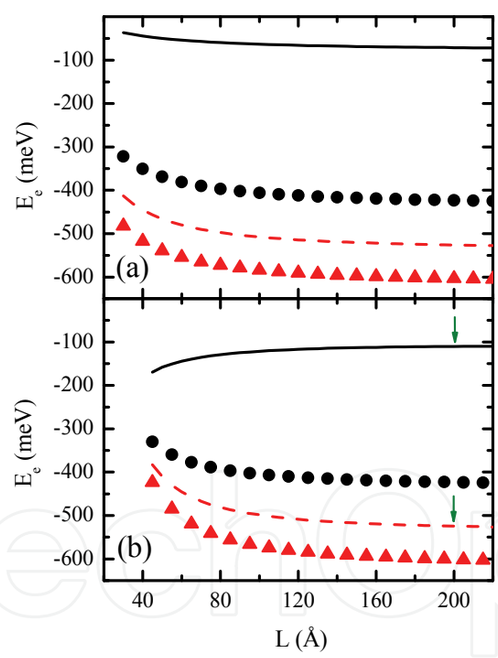

Fig. 2. Electron confinement energies in a cylindrical QWR with a longitudinal GaP/GaAs heterostructure, with interface thickness (a) 0 and (b) 20 Å , as a function of the well width L, for l = 0 (symbols) and l = 1 (curves). Two values of the wire radius R were considered: 35 Å (black, circles, solid) and 75 Å (red, triangles, dashed). The electron wavefunctions for the points indicated by green arrows (L = 200 Å) are plotted in Fig. 4(a).

For abrupt interfaces, a decrease in all energy levels is observed as the well width L is enlarged, similar to the case of quantum wells (Chaves et al., 2007). However, when graded interfaces are taken into account in a R = 35 Å wire, as shown in Fig. 2 (b), the energy of the

electron l = 1 state increases with the well width, for small values of L. This indicates that in this system, such state is now confined at the interfacial regions, so that an enlargement on the well width L further separates the interfaces and increases the confinement energy of the n = 1 state, analogous to the case of the energy levels in double quantum wells. (Ferreira & Bastard, 1997) Conversely, in l = 0 states for R = 35 Å and in all the states shown for R = 75 Å, the same qualitative behavior is observed for abrupt and w = 20 Å interfaces, namely their energies decrease as increasing L, but quantitatively, the presence of graded interfaces still plays an important role, giving a significant blueshift on these energies, specially for small L and large R. For instance, if we consider a L = 45 Å QWR, the energy blueshift due to the graded interfaces is about $\Delta E_e = E_e(w) - E_e(0)$ = 30 meV (105 meV) for l = 0 states in a R = 35 Å (75 Å) QWR. This blueshift in the energy states when non-abrupt interfaces are taken into account has also been predicted in quantum wells, *core-shell* QWR and quantum dots with graded interfaces. (Chaves et al., 2007; Costa e Silva et al. 2006; Caetano et al. 2003) These results are reasonable since, for large wire radius, the radial confinement energy $E_{n,l}^{(\rho)}$ is small, thus the presence of graded interfaces acts like in a quantum well, reducing the confinement region in the heterostructure potential $V^{het}(z)$, hence, enhancing the energy levels. Yet, for smaller values of wire radius, the presence of an interfacial region creates cusps that can confine carriers, as shown in Fig. 1 (b) (solid), which can i) reduce the energy blueshift due to interfaces in this case, or ii) lead to a redshift, as observed for l = 1 when R = 35 Å. Numerical results show that the electron confinement at the interfacial region for lower energy states, as well as the type-I (well) to type-II (barrier) transition in effective potential predicted in previous works (Voon & Willatzen, 2003; Chaves et al., 2008), occurs for small values of R, which can be troublesome for experimental verification of these features. Nevertheless, one could try to find another way to induce these variations on the carriers localization: The main effect produced by reducing the QWR radius is that the carriers wave functions are squeezed towards the wire axis. If a magnetic field is applied parallel to the wire axis, the same effect can be obtained, hence, type-I to type-II transitions and interfacial confinements, which were found for wires with small radii, are expected to be found for high magnetic fields as well.

In order to verify this alternative way of obtaining these effects, in Fig. 3 we study the influence of an applied magnetic field, parallel to the wire axis, on the confinement energies of electrons. The energies of l = 1 states in a GaP/GaAs QWR with R = 42 Å are shown as functions of the well width L, considering (a) w = 0 Å and (b) w = 20 Å. Three values of magnetic field are considered: B = 0 T (blue, dashed), 10 T (red, dotted) and 30 T (black, solid). The states with zero angular momentum l are not shown, for such states have negligible interaction with magnetic fields. From the Hamiltonian of Eq. (2), one can easily verify that l = 1 states are much more affected by increasing this field, since there is an additional term in this Hamiltonian involving the cyclotron frequency w_c and the angular momentum l. For abrupt interfaces (Fig. 3 (a)), the presence of a magnetic field enhances the confinement energies, but gives no appreciable change in qualitative behavior of E_e versus L curves. However, considering graded interfaces (Fig. 3 (b)), these curves are qualitatively different: the energy behavior B = 30 T (black, solid) is crescent as the well width L increases, whereas the opposite behavior is observed for B = 0 T (blue, dashed) and B = 10 T (red, dotted). This can be understood as an interfacial confinement of these states, not induced by reducing the wire radius, as in Fig. 2 (b), but due to the presence of a magnetic field parallel

to the wire axis. It can be demonstrated by our model that, keeping the same interface thickness w = 20 Å, but considering a slightly smaller radius, R = 40 Å , the electron would be already confined at the interface, so that there is no need for applying a magnetic field to observe this kind of confinement if these values are chosen for the parameters of the system. However, with R = 40 Å and a smaller interface thickness w = 15 Å , the electron is confined at the GaAs layer and, in this case, interfacial confinements induced by magnetic fields were also found, but only for B = 30 T, whereas for R = 42 Å and w = 20 Å, we observed that an interfacial confinement for this system occurs already at a B = 20 T magnetic field. Our results also predict that interfacial confinement of l = 1 electrons due to magnetic fields can be found in InP/InAs QWR too, with a slightly larger radius R = 48 Å (not shown in this work). This can be an interesting feature of these systems since, once the QWR is grown its radius is fixed and an external parameter, namely the magnetic field, can just be tuned to obtain an electron confinement at the well or at the interfaces.

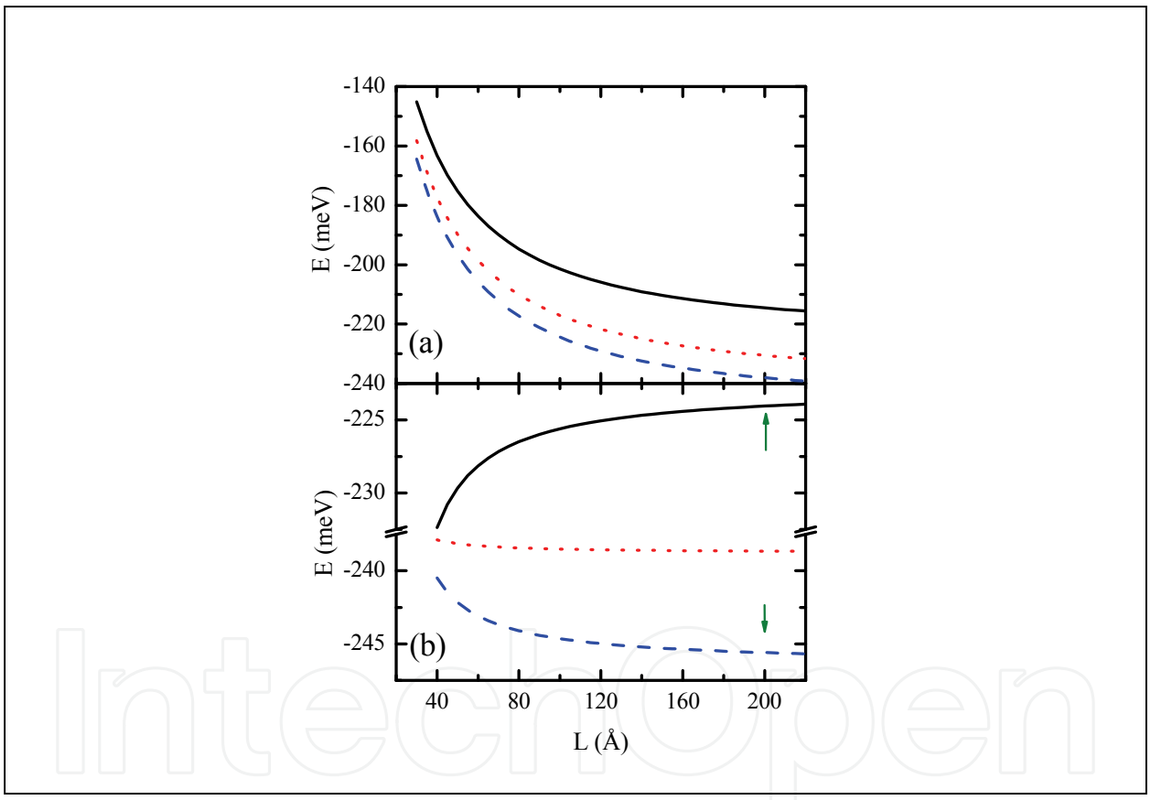

Fig. 3. Electron confinement energies as functions of the well width L for l = 1 states in a cylindrical GaP/GaAs QWR with wire radius R = 42 Å , considering interfaces thicknesses w = 0 (a) and 20 Å (b), under applied magnetic fields B = 0 T (blue, dashed), 10 T (red, dotted) and 30 T (black, solid). The electron wavefunctions for the points indicated by green arrows (L = 200 Å) are plotted in Fig. 4(b).

The interfacial confinement of states in GaP/GaAs QWR can be verified by analyzing the electron wave functions as a function of z in such systems, which is illustrated in Fig. 4, for (1, 1, 1) states for the results marked by arrows in Figs. 2 and 3. In Fig. 4 (a), two values of wire radius are considered, in the absence of magnetic fields, while in (b) the wire radius is

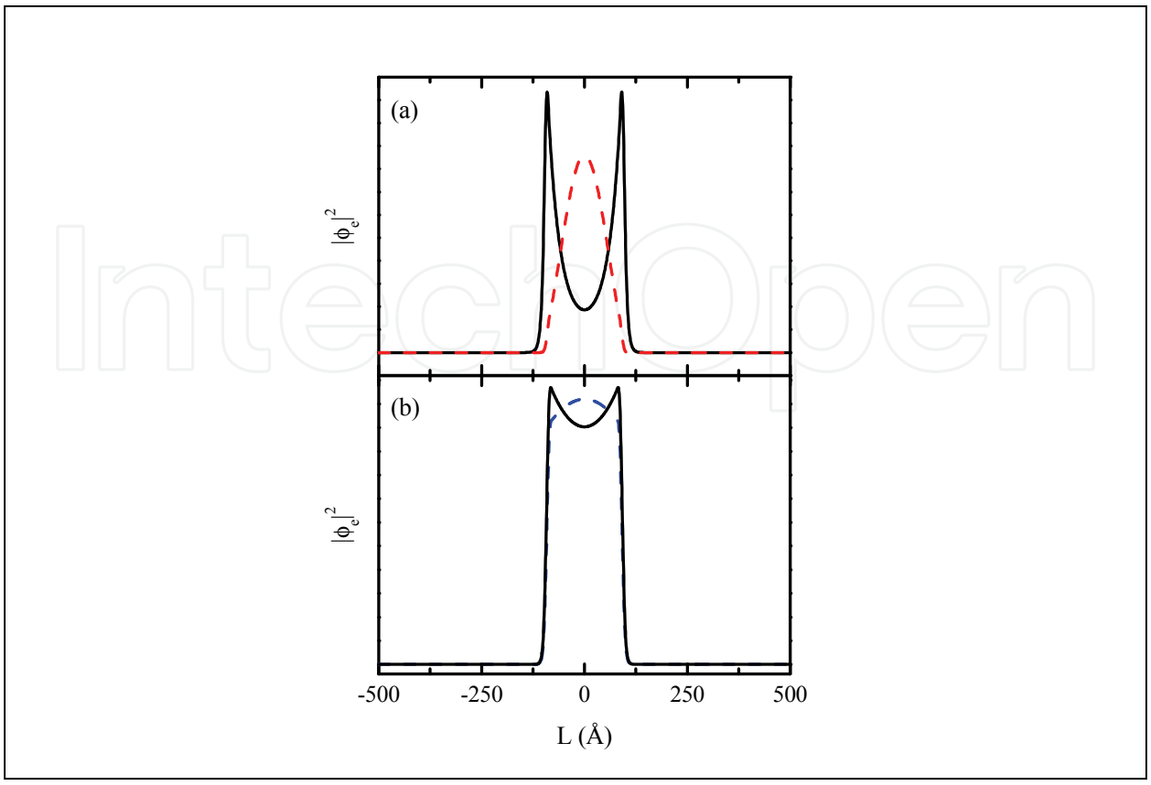

Fig. 4. Electron wave functions for l = 1 states in a cylindrical GaP/GaAs QWR with graded interfaces of w = 20 Å thickness and well width L = 200 Å , as a function of z, considering (a) wire radius R = 35 Å (black, solid) and R = 75 Å (red, dashed) in the absence of magnetic fields; and (b) magnetic fields B = 0 T (blue, dashed) and B = 30 T (black, solid) for a R = 42 Å wire radius.

kept and two values of the magnetic field B are considered. A confinement of l = 1 states is induced when the wire radius is reduced from R = 75 Å (red, dashed) to R = 35 Å (black, solid), as observed in Fig. 4 (a). When a magnetic field is applied, in Fig. 4 (b), the wave function of such states in a R = 42 Å QWR is also altered, and for B = 30 T (black, solid), two peaks at the interfacial regions can be seen. Therefore, we can conclude that, in the presence of graded interfaces, one can obtain confined states at the interfacial regions by reducing the wire radius as well as by increasing the magnetic field intensity.

In Fig. 5, the electron confinement energies are plotted as a function of the well width L, for l = 1 states in InP/InAs/InP QWR with R = 45 Å. For w = 0 Å (Fig. 5(a)), the confinement energies for such a state in the absence of magnetic fields (black, solid) decrease with increasing L, but for B = 10 T (red, dotted) the energy of the (1, 1, 1) is zero for all L, which shows that these states are not confined in z, despite the presence of a heterostructure. This indicates that the barrier like potential due to the radial confinement energy $E_{n,l}^{(\rho)}(z)$, for B = 10 T, is high enough to suppress the contribution of the heterostructure potential in $V(z)$ for this system, yielding a type-II effective potential in the case of abrupt interfaces. This suggests that, with a InP/InAs/InP QWR with abrupt interfaces, one could control the electron band offset or even change from a confinement to a scattering potential for non-zero l states, just by setting the external magnetic field. On the other hand, taking account of

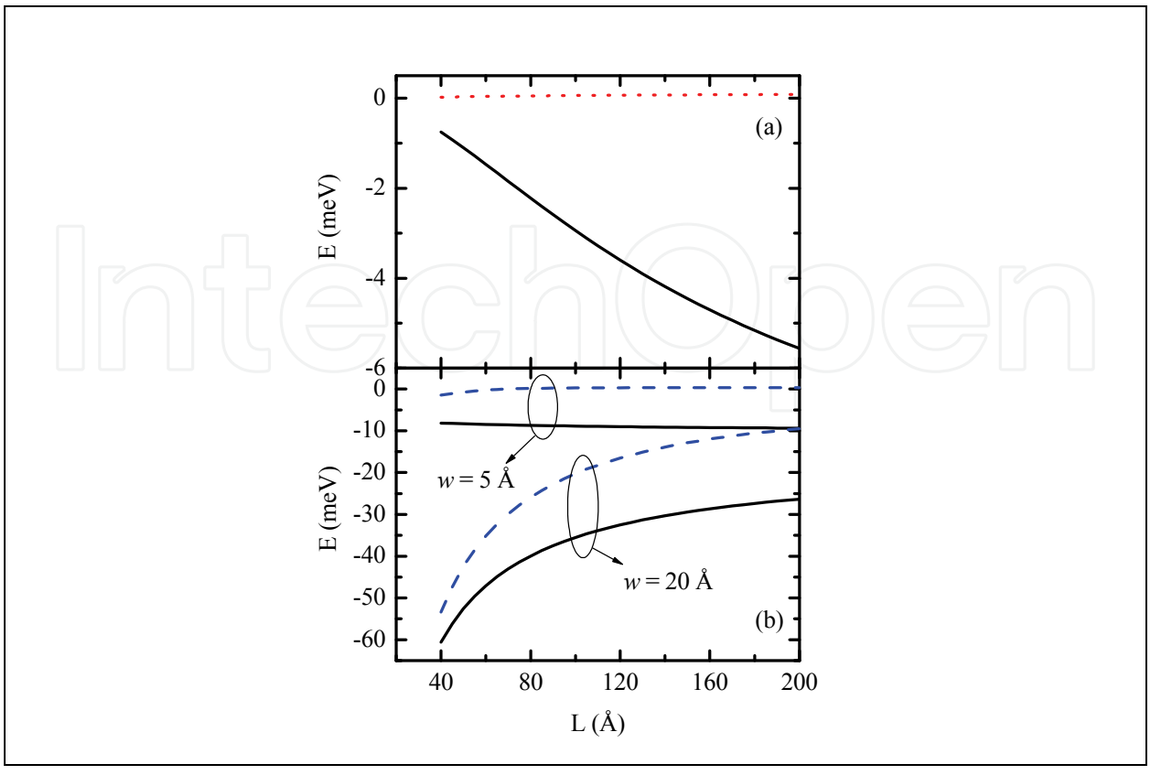

Fig. 5. (a) Electron confinement energies as functions of the well width L for l = 1 states in a cylindrical InP/InAs QWR with wire radius R = 45 Å and abrupt interfaces, under applied magnetic fields B = 0 T (black, solid) and 10 T (red, dotted). (b) The same of (a), but considering graded interfaces of w = 5 and 20 Å, and magnetic fields B = 0 T (black, solid) and 20 T (blue, dashed).

the existence of graded interfaces in real QWR, the results in Fig. 5 (b) show that for larger smooth interfaces (w = 20 Å), the magnetic field does not change the qualitative behavior of l = 1 electrons, which are confined at the interfaces for both B = 0 T (black, solid) and 20 T (blue, dashed). Considering a small interface thickness w = 5 Å, with B = 0 T (black, solid), the electron l = 1 state is confined at the InAs (well) layer and, due to the form of $V(z)$ in this case, it depends weakly on the well width: for L varying from 40 Å to 200 Å considering w = 0 Å, the energy of such a state decreases about 5 meV, whereas for w = 5 Å, it varies only about 1 meV. For a B = 20 T (blue, dashed) magnetic field, considering an interface thickness w = 5 Å, a weak interfacial confinement of (1, 1, 1) electrons is still observed for L lower than 80 Å, while for greater values of L, the barrier on the effective potential is large enough to avoid confinement at the interfaces, leading to a zero energy for such states and an electron localization at the InP layers, just like in a type-II system. Thus, for a perfect type-I to type-II transition induced by a magnetic field in InP/InAs/InP non-abrupt QWR, one would need a R = 45 Å wire with a large InAs layer and small interfaces (< 5 Å), *i. e.* with a very high quality of heterostructure modulation, in order to avoid interfacial confinements. The presence of magnetic fields has been shown to induce interfacial confinement for l = 1 states, because this field enhances the radial confinement energy $E_{n,l}^{(\rho)}(z)$ and then supports this change of localization. However, for l = -1 states, the magnetic field reduces $E_{n,l}^{(\rho)}(z)$, hence,

it would never induce a change from well to interfacial localization of such states. Conversely, there are some cases where the l = -1 electron state is already confined at the interfaces, for instance, in a GaP/GaAs QWR with R = 39 Å and w = 15 Å, and a magnetic field B = 30 T can induce a transition from interfacial to well localization. Such a transition can also be obtained with R = 40 Å and w = 20 Å, but applying a higher magnetic field intensity, B = 35 T.

In present work, as one can verify in Sec. 2, the interfacial region is assumed to be a $XP_{\chi}As_{1-\chi}$ (X = Ga or In) alloy, with a P composition $\chi(z)$ varying linearly along z at the interfaces. The effective masses are then assumed to depend linearly on the composition, but other dependencies on $\chi(z)$, for instance, a linear dependence for the reciprocal effective mass, *i. e.*, $1/m(z) = (1/m_{XP})\,\chi(z) + (1/m_{XAs})[1 - \chi(z)]$ could be considered as well. Straightforward calculations with a simple algebra show that, even for this kind of variation, one can still tailor the system in order to find confining potentials at the interfaces. (nosso artigo)

The study of electron states in the conduction band for the systems we have considered so far can be done by the theoretical model we present in this work, as a good approximation. However, this simple one-band model fails when studying valence band states, because in cases where the wire diameter $2R$ and the heterostructure width L have almost the same dimensions, the lowest valence state is a combination of heavy-hole (HH) and light-hole (LH) states. Indeed, the problem of the confinement of holes in QWR with $2R$ close to L must be solved rather using a 4 x 4 Hamiltonian, which takes into account HH and LH states. Nevertheless, it can be inferred that the critical radii for type-I to type-II transitions, as well as those for interfacial confinements, are not expected to be the same for electrons and holes, since the effective masses of these carriers are completely different in each material and the changes in localization are strongly dependent on the differences between effective masses. In fact, a previous work (Voon et al., 2004) has shown that with a four-band *k.p* based theory one can obtain type-I to type-II transitions also for valence band states in abrupt InGaAs/InP and GaAs/AlAs QWR, and the critical radii they found are different for electrons and holes. Furthermore, considering a GaAs/GaP QWR, changes in valence band states localization would hardly be obtained, due to the small difference between the hole effective masses in GaAs and GaP. However, changes in the electrons localization are found in this system (see Fig. 2(b)). These electron-hole separations might decrease the overlap between their ground state wave functions, which would reduce the probability of an interband transition for such states, a feature that is also commonly found in type-II systems. Thus, a low probability of interband transitions would be observed in cases where the hole remains at the well layer and the electron is confined at the interfaces or vice-versa.

2.2 Double heterostructure

Let us study a different case, where the longitudinal direction presents a double heterostructure, composed by InP and InAs layer. If these materials are disposed as InP/InAs/InP/InAs/InP, the electron will experience a double well structure in z direction in the case where the radial confinement energy is small, that is, when the wire radius is large: the InAs layers will act like confining wells and the InP layers, as barriers. However, as we have discussed earlier, as the wire radius is reduced, the radial confinement energy $E_{n,l}^{(\rho)}(z)$ becomes stronger and reduces the conduction band offset, leading even to a type-I to type-II transition for thin wires. In this section, we will study the double heterostructured

system considering wire radii close to the critical radii that lead to the type-I to type-II transition, so that the InAs layers in this case can act like wells or barriers, depending on the wire radius. As we have the potential in z direction $V(z) = V^{het}(z) + E_{n,l}^{(\rho)}(z)$, we can easily calculate the transmission probabilities T for an electron passing through the double heterostructure, by means of the well known transfer matrix formalism. (Tsu & Esaki, 1973) In all cases studied in this section, we will deal only with ground state electrons for the radial confinement, *i. e.* considering $n = 1$ and $l = 0$.

Figure 6 shows the logarithm of the transmission probability T of the electron as a function of its energy, for three three values of the wire diameter $D = 2R$. The widths of the InP and InAs layers are chosen as L_{InP} = 70 Å and L_{InAs} = 100 Å, respectively. As one can se in the insets of Fig. 6 (a), for abrupt interfaces, the longitudinal effective potential $V(z)$ for these wire diameters is a high double barrier, a very small double barrier and a double well, respectively. Since we have a double barrier for D = 40 Å (black, solid), the transmission probabilities in this case present some peaks which are related to the confined states of the quantum well formed in-between these barriers. When the electron energy reaches one of the eigenenergies of such quantum well, there is a complete transmission of the electron wavefunction, giving rise to the so called resonant tunneling effect. As the diameter of the

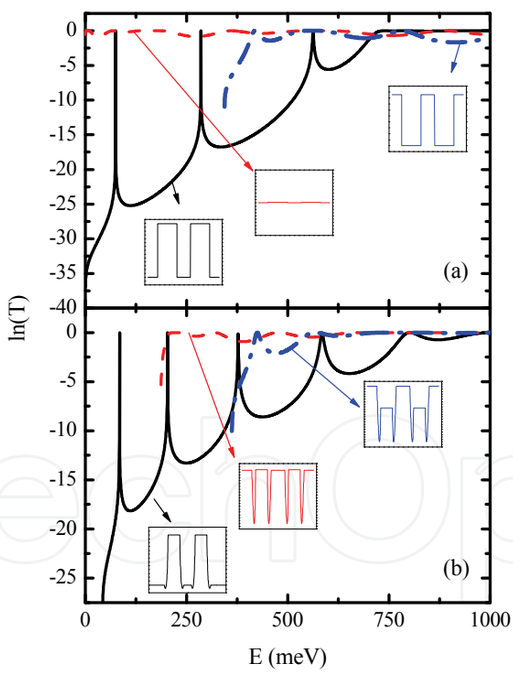

Fig. 6. Transmission probabilities (logarithm) as a function of the electron energy for a QWR with a longitudinal double heterostructure, three values of the wire diameter $D = 2R$: 40 Å (black, solid), 55 Å (red, dashed) and 80 Å (blue, dashed-dotted), considering abrupt (a) and w = 20 Å (b) interfaces. The widths of the InP and InAs layers are chosen as 70 Å and 100 Å, respectively. The insets illustrate a sketch of the longitudinal effective potential $V(z)$ for each wire diameter.

ring increases, the barriers height is reduced and for D = 55 Å (red, dashed) we observe an almost flat conduction band for the electron. As a consequence, for this value of the wire diameter, the electron can be completely transmitted, with $T \simeq 1$, for any value of the electron energy E, as in a free electron case, despite the presence of the longitudinal heterostructure. For larger diameters, as in the D = 80 Å (blue, dashed-dotted) case, the InAs layers become wells and the transmission oscillations are only due to resonant states over the well region, in the continuum. The presence of w = 20 Å interfaces, as shown in Fig. 6 (b), gives rise to some relevant effects: i) the number of resonant tunneling peaks increases, due to the enlargement of the region between the two barriers, and ii) the oscillations in T for higher energies are altered, due to the new form of the interfacial potential.

The barriers width in double heterstructures plays an important role in the resonant tunnelling: as the barrier width becomes larger, the resonant transmission peak becomes narrower and the peak-to-valley difference increases, which is also reflected in the tunnelling time of the resonant states. (Singh, 1993) This is illustrated in Fig. 7 (a), for a QWR with diameter D = 50 Å, considering several values of the InAs layer width L_{InAs} and abrupt interfaces. This diameter is thin enough to make the effective potential present barriers for electrons at the InAs layers, hence, increasing the width L_{InAs} of these layers produces the effects we mentioned due to the enlargement of the barrier width. However, for an interface thickness w = 20 Å, this picture changes, because of the presence of the cusps in the

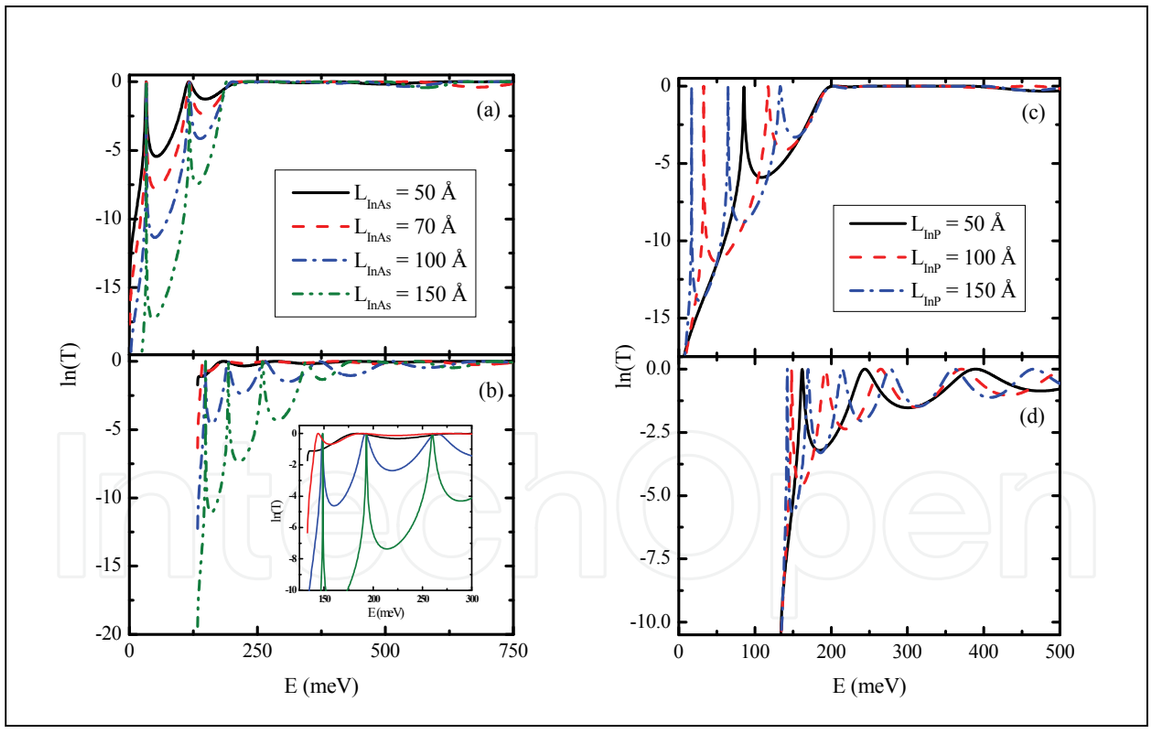

Fig. 7. Transmission probabilities (logarithm) for a 50 Å diameter wire with a double longitudinal heterostructure InP/InAs/InP/InAs/InP considering (a), (b) several values of width of the InAs layers L_{InAs}, while the width of the InP layer is kept the same L_{InP} = 70 Å, and (c), (d) several values of width of the InP layers L_{InP}, while the width of the InAs layer is kept the same L_{InAs} = 100 Å, for abrupt (a), (c) and w = 20 Å (b), (d) interfaces. The inset is a magnification of the results presented in (b).

interfacial region, as shown in Fig. 1. In this case, enlarging the InAs layer, we increase not only the barrier width, but also the separation between these cusps, hence, the effect of increasing L_{InAs} is not simply making the peaks narrower and changing peak-to-valley differences, as one can see in Fig. 7 (b). It can be seen that even the position of the peaks is slightly altered by enlarging L_{InAs} in the non-abrupt case, as highlighted by the inset.
By increasing the width of the InP layers L_{InP} in the D = 50 Å wire that we considered in Fig. 7, we are enhancing the well region and, consequently, more resonant tunnelling peaks are expected to occur, as one can verify in Fig. 7 (c), for abrupt interfaces: while the L_{InP} = 50 Å system (black, solid) has only one sharp peak, two and three peaks are observed for L_{InP} = 100 Å (red, dashed) and 150 Å (blue, dashed-dotted), respectivelly. Figure 7 (d) shows that, for these systems, the different effective potential $V(z)$ created by the presence of w = 20 Å graded interfaces is responsible for changes in the position of the peaks and leads to oscillations in the transmission probability for higher energies.

3. Core-shell quantum wires

As we will investigate the excitonic properties of core-shell quantum wires, we consider a potential in Eq. (1) that includes the electron-hole interaction, so that the Hamiltonian describing the confinement of these carriers now reads $H_{exc} = H_e + H_h + H_{e-h}$, where the single particle Hamiltonian H_i, with i = e (electron) or h (heavy hole), can be straightforwardly derived from Eq. (1) as

$$H_i = -\frac{\hbar^2}{2\rho_i}\frac{d}{d\rho_i}\frac{\rho_i}{m_i^{\parallel}(\rho_i)}\frac{d}{d\rho_i} + \frac{m_i^{\parallel}(\rho_i)\omega_c^2\rho_i^2}{8} + \frac{\hbar^2 l^2}{2m_i^{\parallel}(\rho_i)\rho_i^2} + \frac{l}{2}\hbar\omega_c + V_i^{het}(\rho_i) \tag{6}$$

and the electron hole interaction Hamiltonian H_{e-h} is given by

$$H_{e-h} = -\frac{\hbar^2}{2\mu^{\perp}}\frac{\partial^2}{\partial z^2} - \frac{e^2}{4\pi\varepsilon}\frac{1}{|\vec{r}_e - \vec{r}_h|} \tag{7}$$

where $\mu^{\perp} = 1/m_e^{\perp} + 1/m_h^{\perp}$ is the reduced mass in longitudinal direction and ε is the effective dielectric constant of the media. After a separation of variables, the single particle Hamiltonian H_i describing the confinement of each carrier in the radial direction is diagonalized numerically, by means of a finite differences scheme (Peeters & Schweigert, 1996), whereas a variational procedure is taken for the electron-hole interaction, by considering a Gaussian function

$$Z(z) = \frac{1}{\sqrt{\eta}}\left(\frac{2}{\pi}\right)^{\frac{1}{4}}\exp\left(-\frac{z^2}{\eta^2}\right) \tag{8}$$

as the solution for the z-direction, where η is a variational parameter that minimizes the exciton energy.
We have applied this theoretical model to study $Si/Si_{1-x}Ge_x$ core-shell quantum wires. It has been shown in previous papers that for lower Ge concentrations this heterostructure exhibits a type-I confinement for electrons, but a type-I to type-II transition occurs as the Ge concentration x increases (Kamenev et al., 2005). Then, in this work we study both types of

confinement, for the appropriate Ge concentrations in each case. The material parameters for Si and Ge can be easily found in litterature (Penn et al., 1999) and the parameters of the alloy were obtained by interpolation of those of the pure materials.

3.1 Type-I Si/$Si_{0.85}Ge_{0.15}$ wire

For a type-I system, we solve numerically the Schrödinger equation $H_i\psi_i(\rho_i) = E_i\psi_i(\rho_i)$ to obtain the energy and the radial wavefunctions of each charge carrier, so that the total exciton wavefunction reads $\Psi(\vec{r}) = \left(1/\sqrt{2\pi}\right)\exp[il\theta]\psi_e(\rho_e)\psi_h(\rho_h)Z(z)$. Then we search for η so that $\langle\Psi|H_{exc}|\Psi\rangle = E_e + E_h + E_b(\eta)$ is minimized, with

$$E_b(\eta) = \langle\Psi|H_{e-h}|\Psi\rangle = -\frac{\hbar^2}{2\mu^{\perp}}\int_{-\infty}^{\infty} Z(z)\frac{\partial^2}{\partial z^2}Z(z)dz - \frac{e^2}{4\pi\varepsilon}\int_V \frac{|\psi_e(\rho_e)|^2|\psi_h(\rho_h)|^2 Z^2(z)}{\sqrt{z^2 + |\overrightarrow{\rho_e} - \overrightarrow{\rho_h}|^2}}dV \qquad (9)$$

where the volume element is $dV = \rho_e d\rho_e \rho_h d\rho_h d\theta dz$. Using the Gaussian variational function of Eq. (8), the first integral in Eq. (9) is solved analytically, while the second integral can be simplified, yielding

$$E_b(\eta) = \frac{\hbar^2}{2\mu^{\perp}\eta^2} - \frac{e^2}{4\pi\varepsilon\eta}\sqrt{\frac{2}{\pi}}\int_0^{\infty}|\psi_e(\rho_e)|^2\rho_e\int_0^{\infty}|\psi_h(\rho_h)|^2\rho_h\int_0^{2\pi}\exp(a)K\left(\frac{a}{2}\right)d\rho_e d\rho_h d\theta \qquad (10)$$

with $a = -2|\overrightarrow{\rho_e} - \overrightarrow{\rho_h}|/\eta$ and $K(x)$ is the modified Bessel function of the second kind (table of integrals). The remaining integral in Eq. (10) is then performed numerically and, after the minimization, we eventually obtain the total exciton energy as $E_{exc} = E_{gap} + E_e + E_h - E_b$, where E_{gap} is the gap of the core material.

The binding energy (black) and the ground state energy (red) of *e-hh* excitons in $Si/Si_{0.85}Ge_{0.15}$ QWR are shown in Fig. 8 as a function of the wire radius for interface thicknesses w = 0 Å (solid) and 15 Å (dashed). Notice that the binding energy increases as the wire radius increases up to a maximum at ρ_2 = 40 Å (50 Å), for abrupt (graded) interfaces and after this values it starts to decrease. This change of behavior as the wire radius increases is reasonable: reducing the wire radius makes the system seem like bulk Si, where the binding energies are naturally lower. (Ferreira et al., 2002; Costa e Silva et al., 2006) On the other hand, increasing the wire radius enlarges the region of confinement, which is responsible for reducing the binding energy. Hence, there must be some critical value of the radius ρ_2 where the behaviour of the binding energy as a function of the radius changes. For wire radii below this critical value, the inclusion of a graded interface shifts down the binding energies, while the opposite occurs for a larger radii. Numerical results show that for a 30 Å wire radius with interface thickness of w = 15 Å, for example, the binding energy is reduced about 25%, while for wire radii greater than 50 Å there is an average increase in the binding energies of about 5.5%, in relation to the abrupt case. The ground state exciton energy always decreases with the increase of the wire radius, and the inclusion of a graded interface shifts up this energy, especially for thin wires, where these shifts may reach about 30 meV in relation to the abrupt case. Indeed, for a wire radius as large as 120 Å, the inclusion of a 15 Å interface must affect weakly the exciton energy, whereas for a small wire radius, *e. g.* ρ_2 = 40 Å, the dimensions of the wire radius and the

interface thickness are comparable, hence a stronger effect of the interface is expected for the exciton energy in this case.

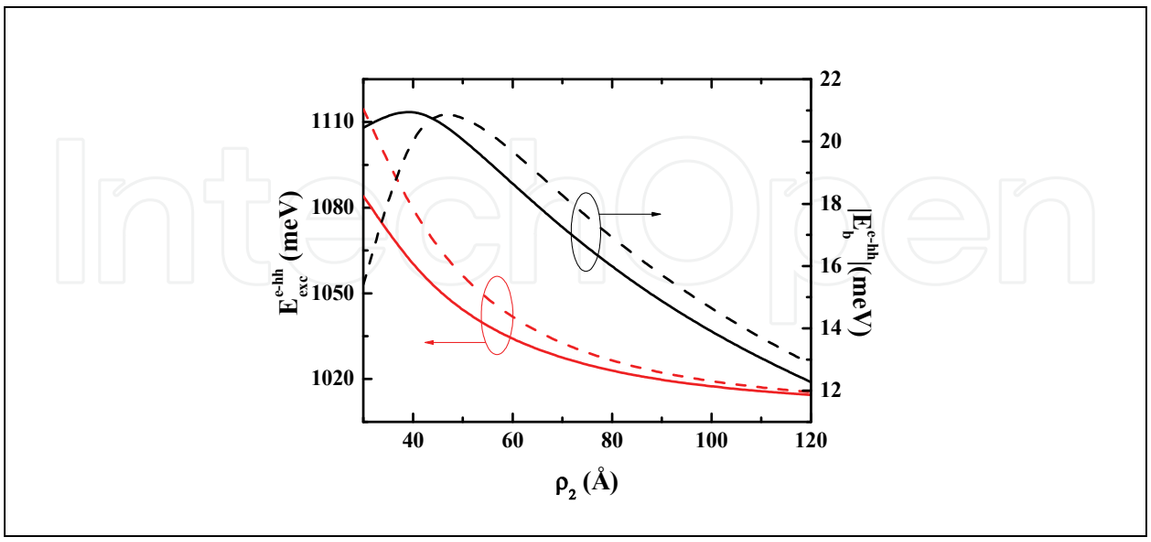

Fig. 8. Binding energy (black, right scale) and ground state exciton energy (red, left scale) of Si/$Si_{0.85}Ge_{0.15}$ type-I wires as a function of the wire radius ρ_2 for abrupt (solid) and w = 15 Å (dashed) interfaces.

The influence of applied magnetic fields on the binding (a) and total (b) ground state exciton energies is presented in Fig. 9 for two values of the wire radius, ρ_2 = 50 Å (black, solid, triangles) and 200 Å (red, dashed, squares), for an abrupt interface (lines) and for w = 15 Å (symbols). The magnetic field does not significantly affect these energies, giving them only small blueshifts of the order of 2 meV, for all values of wire radii considered. Wires with larger radii are more affected by this external field. These results are in good agreement with previous studies in such systems for other materials. (Branis et al., 1993)

3.2 Type-II Si/$Si_{0.70}Ge_{0.30}$ wire

In this case, since the conduction band forms a barrier for electrons, we cannot obtain the radial wavefunction for this carrier just by solving $H_e\psi_e(\rho_e) = E_e\psi_e(\rho_e)$, as we did previously for type-II, for the solution of this equation would lead to a free electron with $E_e = 0$. Hence, for a type-II structure, we must first solve the Schrödinger equation for the hole and use the obtained radial wavefunction $\psi_h(\rho_h)$ to construct an effective Coulombian potential, which is responsible for confining the electron in ρ-direction.
The Schrödinger equation for electrons in this system then reads

$$\left(E_h + H_e + I(\rho_e)\right)\left|\psi_e\right\rangle = E_X\left|\psi_e\right\rangle \tag{11}$$

where the effective Coulomb potential $I(\rho_e) = \langle\psi_h Z\left|H_{e-h}\right|\psi_h Z\rangle$ is obtained from the hole wavefunction and from the Gaussian trial function of Eq. (8) as

$$I(\rho_e) = -\frac{\hbar^2}{2\mu^{\perp}}\int_{-\infty}^{\infty} Z(z)\frac{\partial^2}{\partial z^2}Z(z)\,dz - \frac{e^2}{4\pi\varepsilon}\int_{-\infty}^{\infty}\int_0^{2\pi}\int_0^{\infty}\frac{\left|\psi_h(\rho_h)\right|^2 Z^2(z)}{\sqrt{z^2 + \left|\overrightarrow{\rho_e} - \overrightarrow{\rho_h}\right|^2}}\rho_h d\rho_h d\theta dz \tag{12}$$

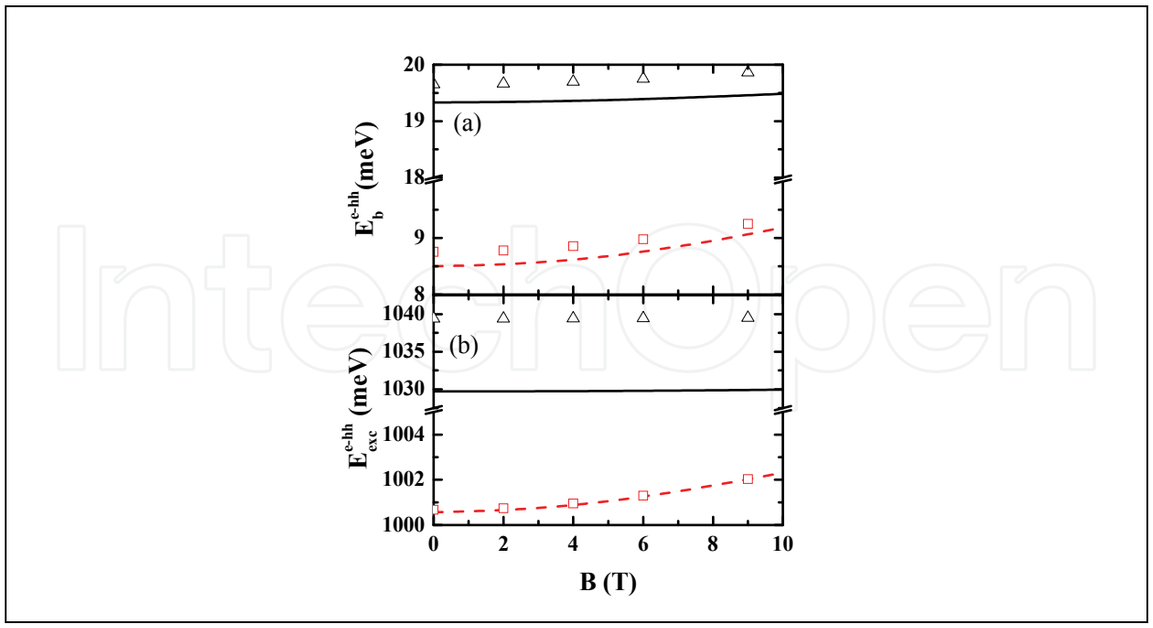

Fig. 9. Binding energy (a) and ground state exciton energies (b) of *e-hh* pairs in Si/SiGe type-I quantum wires as functions of the magnetic field, with w = 0 Å (lines) and w = 15 Å (symbols), for wire radii ρ_2 = 50 Å (black, solid, triangles) and 200 Å (red, dashed, squares).

As for Eq. (9) in the type-I case, the first integral in Eq. (12) can be solved analytically, while the second is simplified, leading to an expression that is similar to what we found in Eq. (10):

$$I(\rho_e) = \frac{\hbar^2}{2\mu^{\perp}\eta^2} - \frac{e^2}{4\pi\varepsilon\eta}\sqrt{\frac{2}{\pi}}\int_0^{\infty}\left|\psi_h(\rho_h)\right|^2\rho_h\int_0^{2\pi}\exp(a)K\left(\frac{a}{2}\right)d\rho_h d\theta \tag{13}$$

Performing this integral numerically, we obtain the effective Coulomb potential for electrons and solve the Schrödinger equation given by Eq. (11). The parameter η is adjusted to minimize E_X and we obtain the total exciton energy by $E_{exc} = E_{gap} + E_X$.

Figure 10 shows the effective confining potential $V_{eff}(\rho_i) = V^{het}(\rho_i) + I(\rho_e)$ (black, solid) and the wave functions (red, dashed) for electrons (top) and holes (bottom) in type-II Si/$Si_{0.70}Ge_{0.30}$ QWR. A depression in the potential for the electron, due to the electron-hole Coulomb interaction, can be clearly seen. This depression is responsible for the electron bound state at the silicon layer near the Si/$Si_{0.70}Ge_{0.30}$ wire, despite the fact that the heterostructure forms a barrier for this carrier.

In Fig. 11, the binding energy (black) and the ground state energy (red) of *e-hh* excitons are plotted as a function of the QWR radius for Si/$Si_{0.70}Ge_{0.30}$ wires with abrupt (solid) and w = 15 Å (dashed) interfaces. Since in type-II systems the electron and hole are localized in different regions of space, the binding energies of type-II wires are lower than those of type I, as one can verify by comparing Figs. 8 and 11. Moreover, these energies always decrease when the wire radius is enlarged, and no change in the behavior of the binding energy versus wire radius curve is observed, contrary to the type-I case studied before. Actually, in the type-II case, in the limit of very thin wires, the system no more seems like bulk Si, but like a bulk system with a localized impurity, since the hole is confined within the thin wire, while the electron is bound to it on the Si layer. Considering a 40 Å wire radius and w = 15 Å

interface thickness, the increase of binding energies is about 12% in relation to the abrupt case, while the total exciton energy is increased by about 20 meV.

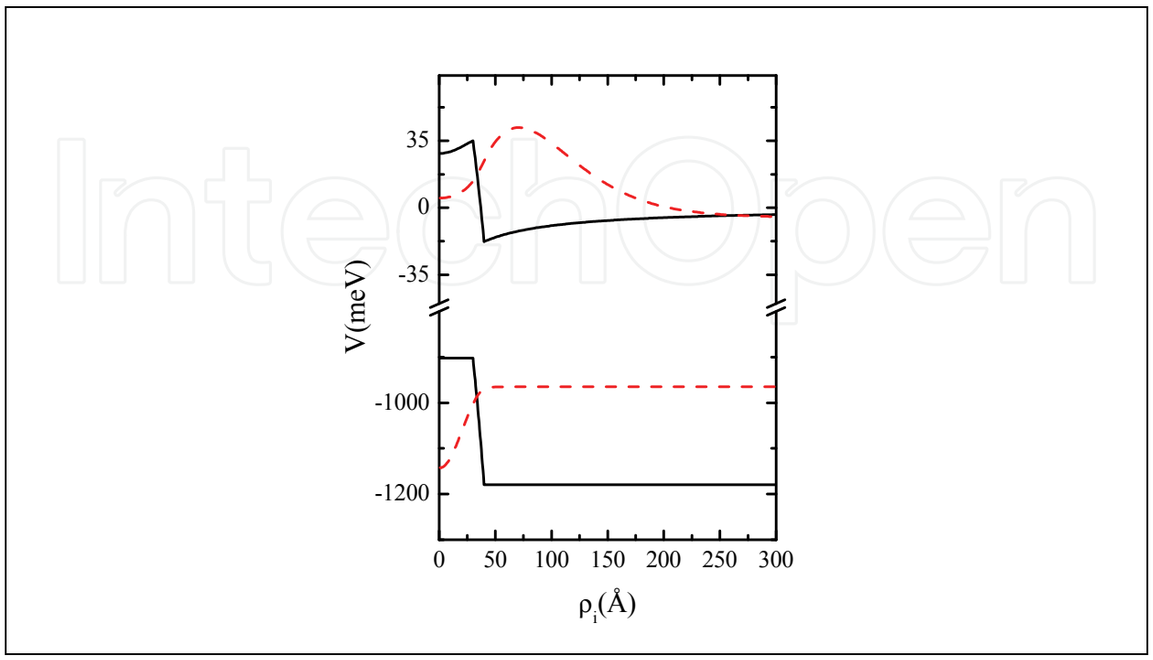

Fig. 10. Confining potentials (black, solid) for electrons (top) and holes (bottom) and their respective wave functions (red, dashed) in a ρ_2 = 40 Å type-II Si/$Si_{0.70}Ge_{0.30}$ QWR.

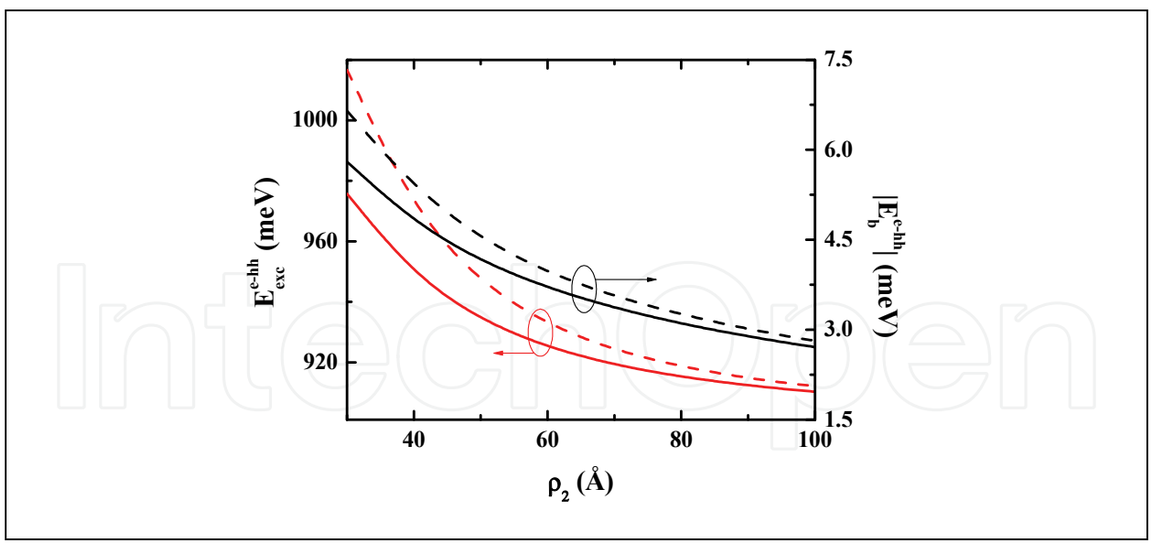

Fig. 11. Binding energy (black, right scale) and ground state energy (red, left scale) of *e-hh* excitons in Si/$Si_{0.70}Ge_{0.30}$ type-II quantum wires as a function of the wire radius, for interfaces thicknesses *w* of 0 Å (solid) and 15 Å (dashed).

The influence of a magnetic field parallel to the wire axis on the binding (a) and total exciton energies (b) of abrupt Si/$Si_{0.70}Ge_{0.30}$ type-II QWR is illustrated in Fig. 12, for the ground (solid) and first excited (dashed) states. The split between these two states is large for the

wire with ρ_2 = 50 Å (black), but it is reduced as the wire radius increases, becoming very small for a 150 Å (red) wire radius, especially for the total exciton energy (b). As the magnetic field increases, the hole angular momentum remains zero in the ground state, but the angular momentum of the electron ground state changes almost periodically, leading to the energy oscillations observed in Fig. 12. Such oscillations can be compared to those observed in quantum rings, as a consequence of the Aharonov-Bohm (AB) effect, and the periodicity of these oscillations depends on the wire radius. (Chaves et al., 2008) The fact that, for the ground state, the hole angular momentum remains zero while the electron

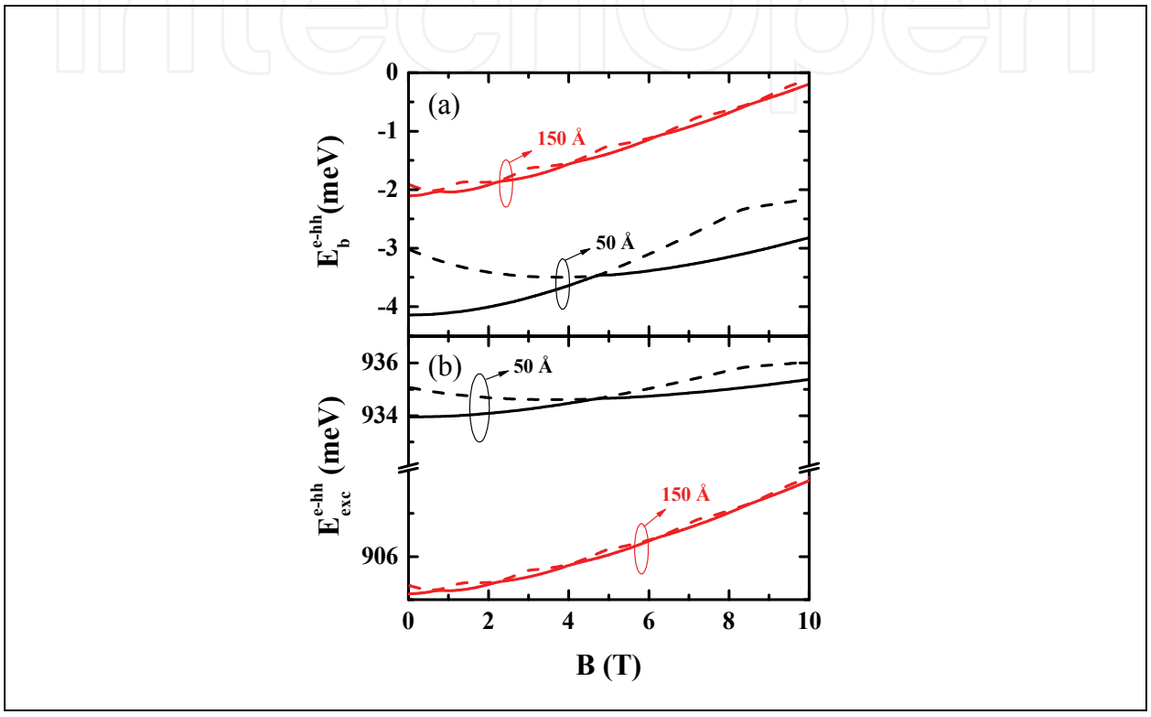

Fig. 12. Binding energies (a) and total exciton energies (b) of *e-hh* excitons in $Si/Si_{0.70}Ge_{0.30}$ type-II QWR as a function of the magnetic field for 50 Å and 150 Å wire radii, with abrupt interfaces. Solid lines are related to ground state excitons, while dotted lines are first excited states.

angular momentum changes as B increases is reasonable, since only the electrons in this system are localized around the wire, which causes the magnetic field to push the electron towards the barrier, giving rise to a change in l in each electron state, because this is energetically more favorable. Since the holes are localized inside the wire, they do not undergo any change in their angular momentum for the ground state. Aharonov-Bohm oscillations in the photoluminescence peaks of type-II stacked quantum dots have been reported recently in experimental works in literature. It has been suggested that the observation of this effect can be a useful tool for proving the radius of the system with a good resolution. (Sellers et al., 2008)

The periodicity of the Aharonov-Bohm oscillations in our results exhibits small changes as the magnetic field increases, in contrast to the oscillations observed in the energy spectrum of quantum-ring structures, where this periodicity is constant and well defined. (Szafran et al., 2004) As one can observe in Fig. 12, the periodicity clearly depends on the wire radius and,

consequently, on the area enclosed by the ring-like potential, as usual for the Aharonov-Bohm effect. Hence, small changes in the periodicity of the electron energy oscillations are expected even for a constant wire radius, because increasing the magnetic field squeezes the hole wave function towards the wire axis, reducing the area enclosed by the effective Coulomb potential for electrons, implying in a larger periodicity for stronger magnetic fields.

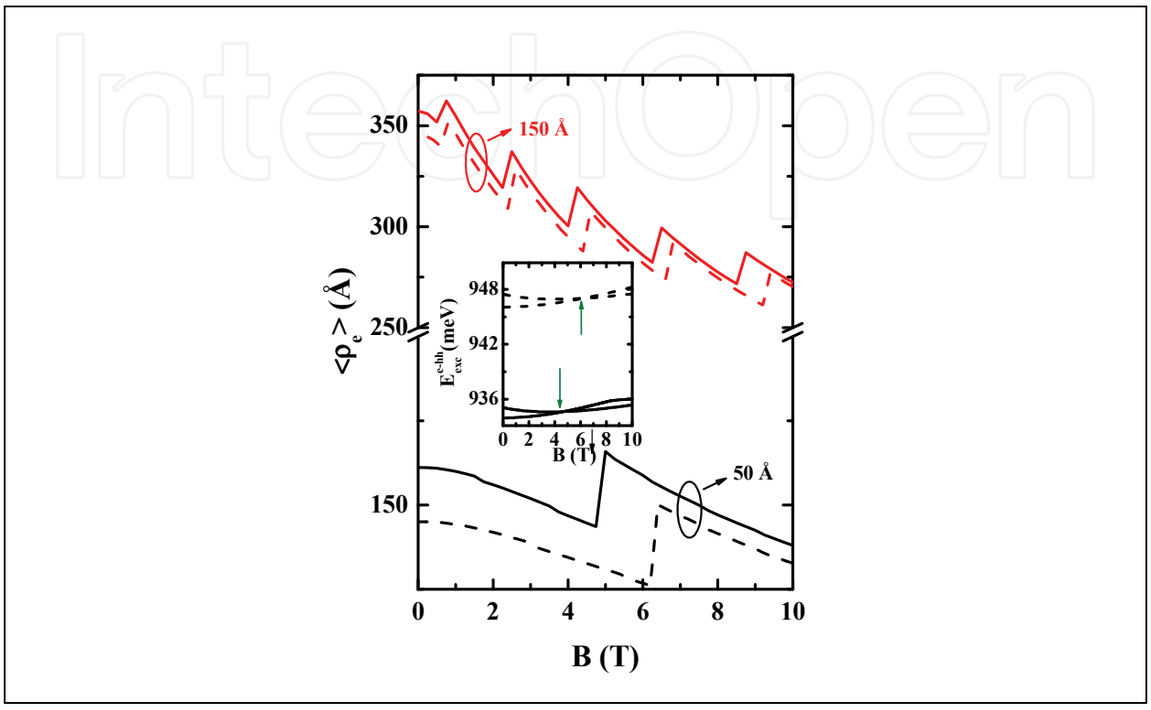

Fig. 13. Average radius of the electron ground state in $Si/Si_{0.70}Ge_{0.30}$ type-II QWR as a function of the magnetic field, for 50 Å (black) and 150 Å (red) wire radii, considering w = 0 Å (solid) and w = 15 Å (dashed). Inset: Exciton energy dependence with the applied magnetic field, for the ground and first excited states of a 50 Å QWR radius with w=0 Å (solid) and w = 15 Å (dashed). The green arrows highlight the angular momentum transition points.

The changes in the periodicity of the angular momentum transitions can be seen in Fig. 13, which illustrated the average radius of the electron ground state $\langle\rho_e\rangle$ as a function of the applied magnetic field, for wire radii 50 Å (black) and 150 Å (red) with abrupt (solid) and w = 15 Å (dashed) interfaces. Since the electron angular momentum is changing almost periodically with the magnetic field, and due to the fact that wave functions for states with a larger modulus of angular momentum are more extensive than those for l = 0, one can expect that the electron average radius $\langle\rho_e\rangle$ will also oscillate as a function of B. When the magnetic field pushes the electron towards the $Si_{1-x}Ge_x$ layer, its average radius decreases until a change of angular momentum occurs, when l assumes a higher modulus value, which implies a more spread electron wave function, as one can verify in Fig. 13. The inset shows the exciton energies related to a 50 Å QWR radius, for ground and first excited states, where a difference between the angular momentum transition points for abrupt (solid) and non-abrupt (dashed) interfaces, highlighted by the green arrows, can be easily seen. This difference, which is also reflected in the electron average radius, is expected to occur, since the inclusion of such an interface reduces the effective radius of the quantum wire potential.

The influence of graded interfaces on the transition points of AB oscillations can be observed even for larger radii. For a 150 Å wire radius with an abrupt interface, the fifth electron angular momentum transition occurs in a magnetic field B about 8.75 T, while for a w = 15 Å interface it occurs at B = 9.4 T. For a smaller radius, *e. g.* 50 Å, this effect is stronger: the first transition occurs at B = 5 T for an abrupt interface, whereas for w = 15 Å it occurs at B = 6.4 T. An exciton energy blueshift also appears due to the inclusion of graded interfaces, as one can observe in the inset of Fig. 13, which is consistent with earlier results of Fig. 11 (red).

3.3 Type-II Si/$Si_{0.70}Ge_{0.30}$ core-multi-shell structures

The growth of Si/SiGe core-multi-shell structures have been reported in literature (Lauhon et al., 2002) and the theoretical model presented in the last session can be straightforwardly adapted to describe such radial heterostructures. An interesting case to be studied is the system composed by a Si core wire, surrounded by a layer (internal shell) of $Si_{1-x}Ge_x$ and covered by a second layer (external shell) of Si. We consider that for a Ge concentration x = 0.30 this system exhibits a type-II potential for electrons in the conduction band, as in the case of core-shell wires we studied and $Si/Si_{1-x}Ge_x$ quantum wells in literature (Penn et al., 1999).

The type-II $Si/Si_{1-x}Ge_x/Si$ core-multi-shell quantum wires have an interesting feature: the $Si_{1-x}Ge_x$ layer forms a well which confine the holes in the internal shell. However, for electrons, this layer is a barrier; thus, the electron must be confined either in the external Si shell, or in the internal Si core. These two situations are expected to lead to completely different situations of the system. For example, in Fig. 14 (a) we show the dependence of the electron-hole binding energy on the core radius ρ_1, considering w = 15 Å interfaces, for some values of the $Si_{1-x}Ge_x$ shell width S. It is observed that the energy increases with ρ_1 until a critical value of this parameter is reached. After this value, the energy starts to decrease. The results for abrupt interfaces (dotted lines) show the same qualitative behavior, although the critical radii in the abrupt case are slightly altered. The behavior of the binding energy as a function of ρ_1 in the first part (for smaller core radius) can be compared to the one of the confinement energy as a function of the average radius in a quantum ring with finite dimension (Song & Ulloa, 2001). In the second part (for larger core radius), these results resemble those found for the binding energy in a type-II wire in Fig. 11 (red). Indeed, if one analyzes the electron average radius $< \rho_e >$ in Fig. 14 (b), one observes that an abrupt transition occurs in these critical core radii, where the electron changes its radial position. A further analysis of this intriguing situation is made in Figs. 14 (c) and (d), where the electron (blue, solid) and hole (red, dashes) wave functions are presented, along with the effective electron confinement potential, for a shell width S = 100 Å and ρ_1 = 100Å (c) and 270 Å (d). Notice that the electron wave function jumps from the external Si shell towards the Si core when the core radius is increased, leading to the change we observed in the binding energies behavior.

The electron confinement in the external shell can lead to rather interesting features in the presence of an applied magnetic field parallel to the wire axis. As the magnetic field intensity increases, the hole confinement energy is expected to present AB oscillations, since this carrier is confined within the internal shell. As the electron is in the external shell for smaller core radii, one can expect that its energy will also exhibit AB oscillations. However, the magnetic field pushes the electron towards the center, which is also a Si layer, thus, for higher magnetic field intensities, the transition from the electron confinement at the external layer to the Si core is also observed and, once the electron is in the core for higher magnetic fields, its energy can not exhibit AB oscillations anymore. Our preliminary results show that

for a core radius ρ_1 = 200 Å and an internal layer width S = 100 Å, a magnetic field B = 0.8 T is enough to induce the electron confinement transition from the external shell to the Si core.

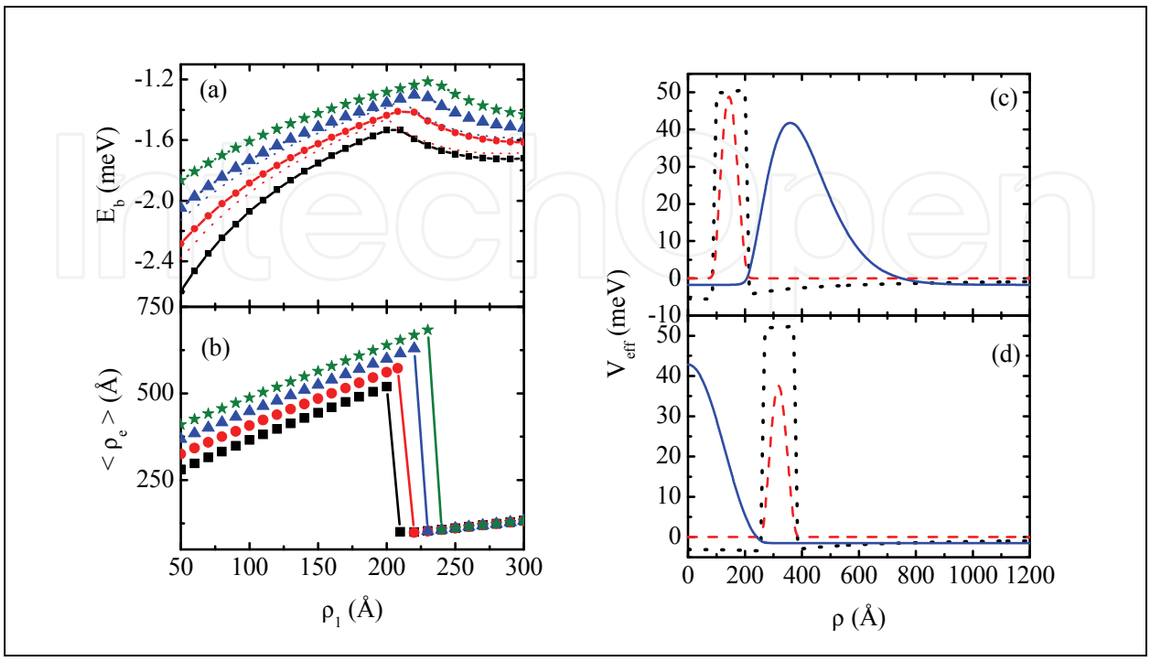

Fig. 14. Binding energy (a) and electron average radius (b) as a function of the core radius for a core-multi-shell structure with w = 15 Å interfaces, considering the internal shell width S as 50 Å (black squares), 75 Å (red circles), 100 Å (blue triangles) and 125 Å (green stars). Dotted lines are the results for abrupt interfaces in the 75 Å and 100 Å cases, while solid lines are just a guide for the eye. The electron (blue, solid) and hole (red, dashed) wave functions, as well as the electron effective potential (black, dotted) for S = 100 Å are shown for ρ_1 = 100Å (c) and 270 Å (d).

4. Conclusion

We have made a theoretical investigation of the electronic properties of two well known types of quantum wire: core-shell and longitudinally heterostructured quantum wires. In both cases, our results show that the existence of graded interfaces between materials can be responsible for significant fluctuations in the confinement energies, for a change in the qualitative behaviour of the wavefunctions and can even affect the excitonic properties of these systems.

For QWR with longitudinal heterostructures, we have shown that, due to the dependence of the radial confinement energy on the carriers effective masses, which are different for each material that compounds the heterostructure, this energy acts like an additional potential in the longitudinal direction, playing an important role on the carriers confinement in this direction. For abrupt interfaces, our results show that one can tune the conduction band offset by either growing a sample with a different radius or changing an applied magnetic field parallel to the wire axis. In this context, even a type-I to type-II transition for the electron longitudinal confinement can be observed by changing these parameters. In the presence of graded interfaces, we have shown that for wider diameters of the QWR, the

electron confinement energies are blueshifted, while for smaller radii, an interfacial localization of the electron can be observed. The critical radii where the changes in the electron and hole localization occur are not expected to be the same; as a consequence, the overlap between the wave functions of these carriers can be small, leading to a low probability of interband transitions in these cases. In addition, significant qualitative changes on the electron transmission probabilities are observed for a longitudinal double heterostructure when non-abrupt interfaces are taken into account. Such changes can be reflected on the experimental observation of the electric current in longitudinally heterostructured QWR, which is left as a suggestion for future experimental research on these structures.

We have also studied $Si/Si_{1-x}Ge_x$ core-shell QWR, which can present type-I or type-II band alignments for electrons, depending on the Ge concentration x in the core. Our results show that the existence of graded interfaces affects significantly the binding and total exciton energies, especially for smaller wire radii, in both type-I and type-II cases. For the type-I structure, as electrons and holes are both confined in a thin quasi-one-dimensional wire, the excitonic properties are not greatly affected by the presence of an axially applied magnetic field. On the other hand, in type-II systems, the hole remains in the core region, whereas the electron is confined by Coulomb interaction with the hole at the shell region, surrounding a barrier like potential produced by the conduction bands mismatch between the core and shell materials. In this situation, as the intensity of an applied magnetic field parallel to the wire axis increases, AB oscillations are observed in the excitonic properties of the system. The period of such oscillations undergoes small changes for stronger magnetic fields, due to the shrinking of the hole in the radial direction induced by the field. Furthermore, although the exciton energy blueshift due to graded interfaces is very small for large wire radii, the presence of such interfaces in the type-II case is also responsible for a change in the angular momentum transition points of the AB oscillations, which can be observed even for wider diameters of the wire. A type-II core-multi-shell structure, where the hole is confined in the internal (first) shell, is also studied. We have shown that, depending on the core radius, the electron can be confined either on the external (second) shell or in the Si core, and the behaviour of the exciton energies as a function of the wire radius for each of these cases is qualitatively different. Such a transition between the electron confinement in the core or in the external shell regions can also be obtained by increasing the intensity of an applied magnetic field in the axial direction. The growth of core-multi-shell Si/SiGe QWR has been already reported in the literature, and our theoretical results show that such structures are very versatile, for one can obtain a system where the hole is in the internal shell, while the electron can be in another shell or in the core, depending on the core radius of the sample or simply by adjusting an external field.

5. References

Li, E. H. (2000). Material parameters of InGaAsP and InAlGaAs systems for use in quantum well structures at low and room temperatures. *Physica E,* Vol. 5, 215-273

Voon, L. C. L. Y. & Willatzen, M. (2003). Electron states in modulated nanowires. *Journal of Applied Physics,* Vol. 93, No. 12, (June 2003) 9997-10000

Chaves, A.; Costa e Silva, J.; Freire, J. A. K. & Farias, G. A. (2007). Excitonic properties of type-I and type-II $Si/Si_{1-x}Ge_x$ quantum wells. *Journal of Applied Physics,* Vol. 101, No. 11, (June 2007) 113703

Costa e Silva, J.; Chaves, A.; Freire, J. A. K.; Freire, V. N. & Farias, G. A. (2006). Theoretical investigation of excitons in type-I and type-II $Si/Si_{1-x}Ge_x$ quantum wires. *Physical Review B,* Vol. 74, No. 8, (August 2007) 085317

Caetano, E. W. S.; Mesquita, M. V.; Freire, V. N. & Farias, G. A. (2003). Strong graded interface related exciton energy blueshift in InGaN/GaN quantum dots. *Physica E,* Vol. 17, (April 2003) 22-23

Ferreira, R. & Bastard, G. (1997). Tunneling and relaxation in semiconductor double quantum wells. *Reports on Progress in Physics,* Vol. 60, No. 3, (March 1997) 345-387

Chaves, A.; Freire, J. A. K. & Farias, G. A. (2008). Grading effects in semiconductor nanowires with longitudinal heterostructures. *Physical Review B,* Vol. 78, No. 15, (October 2008) 155306

Voon, L. C. L. Y.; Lassen, B.; Melnik, R. & Willatzen, M. (2004). Prediction of barrier localization in modulated nanowires. *Journal of Applied Physics,* Vol. 96, No. 8, (October 2004) 4660-4662

Tsu, R. & Esaki, L. (1973). Tunneling in a finite superlattice. *Applied Physics Letters,* Vol. 22, No. 11, (June 1973) 562-564

Singh, J. (1993). *Physics of Semiconductors and Their Heterostructures,* McGraw-Hill Inc., ISBN: 0-07-057607-6

Peeters, F. M. & Schweigert, V. A. (1996). Two-electron quantum disks. *Physical Review B,* Vol. 53, No. 3, (January 1996) 1468-1474

Kamenev, B. V.; Tsybeskov, L.; Baribeau, J.-M. & Lockwood, D. J. (2005). Coexistence of fast and slow luminescence in three-dimensional $Si/Si_{1-x}Ge_x$ nanostructures. *Physical Review B,* Vol. 72, No. 19, (November 2005) 193306

Penn, C.; Schaffler, F.; Bauer, G. & Glutsch, S. (1999). Application of numerical exciton-wave-function calculations to the question of band alignment in $Si/Si_{1-x}Ge_x$ quantum wells. *Physical Review B,* Vol. 59, No. 20, (May 1999) 13314-13321

Ferreira, E. C.; da Costa, J. A. P.; Freire, J. A. K.; Farias, G. A. & Freire, V. N (2002). Interface related effects on confined excitons in $GaAs/Al_xGa_{1-x}As$ single quantum wells. *Applied Surface Science,* Vol. 190, No. 1-4, (May 2002) 191-194

Branis, S. V.; Li, G. & Bajaj, K. K. (1993). Hydrogenic impurities in quantum wires in the presence of a magnetic field. *Physical Review B,* Vol. 47, No. 3, (January 1993) 1316-1323

Chaves, A.; Costa e Silva, J.; Freire, J. A. K. & Farias, G. A. (2008). The role of surface roughness on the electron confinement in semiconductor quantum rings. *Microelectronics Journal,* Vol. 39, No. 3-4, (March-April 2007) 455-458

Sellers, I. R.; Whiteside, V. R.; Kuskovsky, I. L.; Govorov, A. O. & McCombe, B. D. (2008). Aharonov-Bohm excitons at elevated temperatures in type-II ZnTe/ZnSe quantum dots. *Physical Review Letters,* Vol. 100, No. 13, (April 2008) 136405

Szafran, B.; Peeters, F. M. & Bednarek, S. (2004). Electron spin and charge switching in a coupled quantum dot-quantum ring system. *Physical Review B,* Vol. 70, No. 12, (September 2004) 125310

Lauhon, L. J.; Gudiksen, M. S.; Wang, D. & Lieber, C. M. (2002). Epitaxial core-shell and core-multishell nanowire heterostructures. *Nature,* Vol. 420, (November 2002) 57-61

Song, J. & Ulloa, S. E. (2001). Magnetic field effects on quantum ring excitons. *Physical Review B,* Vol. 63, No. 12 (March 2001) 125302

Nanowires

Edited by Paola Prete

ISBN 978-953-7619-79-4
Hard cover, 414 pages
Publisher InTech
Published online 01, February, 2010
Published in print edition February, 2010

This volume is intended to orient the reader in the fast developing field of semiconductor nanowires, by providing a series of self-contained monographs focusing on various nanowire-related topics. Each monograph serves as a short review of previous results in the literature and description of methods used in the field, as well as a summary of the authors recent achievements on the subject. Each report provides a brief sketch of the historical background behind, the physical and/or chemical principles underlying a specific nanowire fabrication/characterization technique, or the experimental/theoretical methods used to study a given nanowire property or device. Despite the diverse topics covered, the volume does appear as a unit. The writing is generally clear and precise, and the numerous illustrations provide an easier understanding of the phenomena described. The volume contains 20 Chapters covering altogether many (although not all) semiconductors of technological interest, starting with the IV-IV group compounds (SiC and SiGe), carrying on with the binary and ternary compounds of the III-V (GaAs, AlGaAs, GaSb, InAs, GaP, InP, and GaN) and II-VI (HgTe, HgCdTe) families, the metal oxides (CuO, ZnO, ZnCoO, tungsten oxide, and PbTiO3), and finishing with Bi (a semimetal).

How to reference

In order to correctly reference this scholarly work, feel free to copy and paste the following:

G. A. Farias, J. S. de Sousa and A. Chaves (2010). Quantum Confinement in Heterostructured Semiconductor Nanowires with Graded Interface, Nanowires, Paola Prete (Ed.), ISBN: 978-953-7619-79-4, InTech, Available from: http://www.intechopen.com/books/nanowires/quantum-confinement-in-heterostructured-semiconductor-nanowires-with-graded-interface

INTECH
open science | open minds

InTech Europe
University Campus STeP Ri
Slavka Krautzeka 83/A
51000 Rijeka, Croatia
Phone: +385 (51) 770 447
Fax: +385 (51) 686 166
www.intechopen.com

InTech China
Unit 405, Office Block, Hotel Equatorial Shanghai
No.65, Yan An Road (West), Shanghai, 200040, China
中国上海市延安西路65号上海国际贵都大饭店办公楼405单元
Phone: +86-21-62489820
Fax: +86-21-62489821

IntechOpen